
LANTERN: A MACHINE LEARNING FRAMEWORK FOR LIPID NANOPARTICLE TRANSFECTION EFFICIENCY PREDICTION

Asal Mehradfar^{1,†,*}, Mohammad Shahab Sepehri^{1,†,*}, Jose Miguel Hernandez-Lobato², Glen S. Kwon³, Mahdi Soltanolkotabi¹, Salman Avestimehr¹, and Morteza Rasoulianboroujeni^{3,4,*}

¹Department of Electrical and Computer Engineering, University of Southern California, Los Angeles, CA

²Department of Engineering, University of Cambridge, Cambridge, UK

³Pharmaceutical Sciences Division, School of Pharmacy, University of Wisconsin-Madison, Madison, WI

⁴Department of Pharmaceutical Sciences, Gatton College of Pharmacy, East Tennessee State University, Johnson City, TN

*Corresponding authors: mehradfa@usc.edu, sepehri@usc.edu, rasoulianbor@etsu.edu

ABSTRACT

The discovery of new ionizable lipids for efficient lipid nanoparticle (LNP)-mediated RNA delivery remains a critical bottleneck for RNA-based therapeutics development. Recent advances have highlighted the potential of machine learning (ML) to predict transfection efficiency from molecular structure, enabling high-throughput virtual screening and accelerating lead identification. However, existing approaches are hindered by inadequate data quality, ineffective feature representations, low predictive accuracy, and poor generalizability. Here, we present LANTERN (Lipid nANoparticle Transfection Efficiency pRedictionN), a robust ML framework for predicting transfection efficiency based on ionizable lipid representation. We benchmarked a diverse set of ML models against AGILE, a previously published model developed for transfection prediction. Our results show that combining simpler models with chemically informative features, particularly count-based Morgan fingerprints, outperforms more complex models that rely on internally learned embeddings, such as AGILE. We also show that a multi-layer perceptron trained on a combination of Morgan fingerprints and Expert descriptors achieved the highest performance ($R^2 = 0.8161$, $r = 0.9053$), significantly exceeding AGILE ($R^2 = 0.2655$, $r = 0.5488$). We show that the models in LANTERN consistently have strong performance across multiple evaluation metrics. Thus, LANTERN offers a robust benchmarking framework for LNP transfection prediction and serves as a valuable tool for accelerating lipid-based RNA delivery systems design. Our code and dataset are publicly available for reproducibility at <https://github.com/AsalMehradfar/LANTERN>.

1 Introduction

RNA therapy holds significant promise for treating diseases by introducing exogenous nucleic acids, such as mRNA, siRNA, and ASOs, to control gene expression in target cells. The FDA's approval of ONPATRO™ in 2018 and Givosiran in 2019, followed by the success of LNP-delivered mRNA vaccines against COVID-19, has firmly established the commercial and clinical viability of RNA therapeutics [1].

RNA therapies rely heavily on delivery systems to overcome biological barriers and reach specific tissues and cells to elicit a therapeutic response [2]. LNPs represent a novel class of non-viral delivery vectors whose efficiency and versatility have been broadly validated by the clinical success of ONPATRO™ and SARS-CoV-2 mRNA vaccines, including Moderna's Spikevax and Pfizer/BioNTech's Comirnaty. LNPs are now considered superior to viral vectors, which pose challenges in clinical applications due to immunogenicity, production costs, and biosafety concerns [3].

Among the four lipid components comprising lipid nanoparticles, ionizable lipids play a central role in RNA encapsulation, protection against nuclease-mediated degradation, and facilitating intracellular delivery. Within the acidic environment of endosomes, ionizable lipids undergo protonation, leading to endosomal membrane disruption and

[†]These authors contributed equally to this work.

promoting the cytosolic release of mRNA for subsequent protein synthesis [4, 5, 6]. While each lipid in the LNP formulation contributes to overall structural integrity and biological function [7, 8, 9, 10, 11, 12], the molecular structure and physicochemical properties of ionizable lipids are particularly influential in determining transfection efficiency.

Despite their importance, the precise structure–function relationships governing ionizable lipid performance remain poorly understood, necessitating the empirical screening of large lipid libraries to identify high-performing candidates [13, 14, 15, 16, 17]. The enormous chemical space, encompassing billions of potential ionizable lipid structures, renders exhaustive experimental synthesis and evaluation infeasible. While combinatorial chemistry, including multi-component reaction strategies, enables high-throughput synthesis of diverse lipid libraries [13, 18, 19], these approaches remain time-consuming and resource-intensive [20]. Moreover, the success rate in identifying highly effective formulations is low. For example, Li et al. [13] synthesized 720 ionizable lipids using a three-component reaction system combining 72 head groups and 10 lipid tails via a nitro ricinoleic acrylate (NRA) linker. Despite this diversity, more than 80% of the formulations showed minimal or no transfection when delivering mLuc mRNA to A549 cells, highlighting the challenges in discovering functional ionizable lipid structures.

Given the challenges of experimentally designing and screening new ionizable lipids, virtual high-throughput screening (vHTS) using machine learning (ML) models trained on limited datasets has emerged as a promising alternative. This approach enables more efficient navigation of the vast chemical space for lipid design. For instance, Ding et al. [21] formulated the transfection prediction problem as a classification task using supervised ML models, including SVM, Random Forest, XGBoost, and Multi-Layer Perceptron (MLP) networks. They compiled a dataset of 572 unique LNPs with experimentally measured luciferase expression in IGROV1 cells based on the study by Liu et al. [14], achieving a classification accuracy of 98% on the test set. This demonstrated the potential of ML in predicting LNP performance and accelerating lipid discovery. Moayedpour et al. [22] further advanced this field by exploring various molecular representations, including RDKit descriptors, circular fingerprints, and pre-trained models such as Grover [23], a customized GCN [24], and MegaMolBART [25]. The latter, fine-tuned on 600,000 lipids from the SwissLipids database, was applied to the dataset curated by Ding et al. [21] and a new dataset created from Liu et al.’s study [14] for binary and four-class transfection classification tasks, respectively. The top-performing approach paired LLM-generated embeddings with a gradient-boosting classifier, achieving an AUC of 0.981 for binary classification and substantial improvements in multi-class predictions.

Although Ding et al. and Moayedpour et al. [21, 22] demonstrated the potential of ML models to predict transfection efficiency based on ionizable lipid structure, both focus primarily on classification tasks, which lack the granularity needed to effectively select optimal candidates for further development. Binary classifiers categorize formulations as satisfactory or unsatisfactory, introducing ambiguity in threshold definition and failing to capture performance variations within the satisfactory category. The four-class classification model proposed by Moayedpour et al. [22] partially addresses this issue for small libraries. However, it still lacks sufficient granularity when applied to large libraries, complicating the identification of top-performing candidates within the highest transfection class.

More recently, Xu et al. [26] introduced the AI-Guided Ionizable Lipid Engineering (AGILE) platform, a graph-based regression model developed to predict the transfection efficiency of ionizable lipids across large-scale chemical libraries. AGILE integrates deep learning with combinatorial chemistry, employing a graph neural network (GNN) encoder derived from the MolCLR architecture [27], which was initially pre-trained via contrastive learning [28] on a dataset of 60,000 virtual lipid structures. To fine-tune the model for quantitative transfection prediction, the authors synthesized a library of 1,200 ionizable lipids using a Ugi-based three-component reaction (3-CR) strategy [18], and experimentally measured their mRNA transfection efficiencies in HeLa and RAW264.7 cell lines. The resulting labeled dataset was used to adapt the pre-trained GNN to the specific task of predicting LNP-mediated transfection efficiency. AGILE evaluates Model performance using a ranking-based approach, in which both predicted and experimentally measured transfection potency values are categorized into six equal percentile bins. Then the model’s ability to correctly classify transfection potency values into each bin was assessed. Under this evaluation scheme, AGILE achieves 41% accuracy in identifying the highest (83rd to 100th percentile) and lowest (0th to 16th percentile) transfection categories, demonstrating moderate capability in prioritizing the most and least effective lipid candidates.

In the present study, we introduce LANTERN (Lipid nANoparticle Transfection Efficiency pRedictionN), a computationally efficient framework for predicting LNP transfection efficiency. We develop LANTERN using a refined version of the ionizable lipid dataset originally published by Xu et al. [26] and used in the AGILE platform. This framework allows training and evaluating diverse predictive models using different molecular representations that capture the relationship between ionizable lipids and their transfection potency in specific cell lines, enabling the rapid identification of promising candidates from large lipid libraries. To facilitate a direct comparison with AGILE, we employed both the ranking-based evaluation scheme used in AGILE and regression-based evaluation metrics, which provide more quantitative and informative insights into model accuracy. We demonstrate that LANTERN offers a comprehensive benchmarking pipeline for the development of accurate predictive models in lipid-based RNA delivery. This framework

advances the broader objective of accelerating therapeutic design by enabling more reliable and efficient computational screening of ionizable lipid candidates.

2 Results

2.1 Overview of LANTERN

To develop a high-accuracy regression model for predicting LNP transfection efficiency based on ionizable lipid structures, it is essential to optimize both the molecular representation and the model architecture. In this study, we conducted a comprehensive analysis of key model components—including molecular representations, model architecture, and data-splitting strategies—using a curated version of the experimental dataset originally used to fine-tune AGILE for transfection prediction in HeLa cells [26]. We then compared the performance of our models to that of AGILE evaluated on the same dataset.

All LANTERN models were either newly implemented or modified for the transfection prediction task, using a unified dataset and consistent preprocessing pipeline. The only exception is AGILE, which serves as a baseline and was evaluated using its official implementation without architectural modifications, retrained on the curated dataset. Detailed implementation and configuration information for all models is provided in Section 4.1. This setup ensures a fair performance comparison while underscoring the flexibility and extensibility of the LANTERN pipeline.

By systematically assessing feature sets, modeling choices, and evaluation methodologies, this study provides insights into the most effective strategies for LNP transfection prediction. To support future research in this domain, we publicly release both the refined dataset and LANTERN, an ML library developed for training and evaluating models for LNP transfection efficiency. Although our primary focus is on LNP transfection, LANTERN is designed as a flexible and extensible framework applicable to a wide range of molecular property prediction tasks.

2.2 Dataset Curation

To ensure consistency in model evaluation, we base our regression models on the HeLa cell transfection experimental data originally reported by Xu et al. [26], which was also used to fine-tune the AGILE model. However, a detailed inspection revealed several discrepancies between the “source data” file published alongside the article¹ and the dataset hosted on GitHub², which AGILE used for fine-tuning. These inconsistencies needed to be resolved to ensure the dataset’s integrity for reliable model training and fair comparative analysis. Two major issues present in the original fine-tuning dataset are as follows:

i) Label Mismatches in SMILES Representations: We identified 235 inconsistencies among the 1,200 data points reported and used in AGILE’s fine-tuning. These inconsistencies stem from errors in mapping SMILES representations to transfection efficiency values, leading to label mismatches. Specifically, the transfection values reported in the original experimental “source data” file do not always correspond to those found in the dataset used to fine-tune AGILE. For instance, lipid A17B11C3, synthesized by combining head group A17 with tails B11 and C3, has a reported transfection efficiency of 0.28 in the experimental data source, whereas in the dataset used for AGILE’s fine-tuning, the same lipid is erroneously assigned a value of 5.43. Similarly, lipid A16B11C3 has a transfection efficiency of 7.69 in the experimental data but is recorded as -0.69 in the dataset used for AGILE’s fine-tuning. These discrepancies appear to originate from systematic errors during the conversion of experimental data into machine-readable SMILES representations, predominantly affecting lipids with B1, B6, B11, or B12 tails.

To rectify this, we manually verified and corrected the dataset by ensuring that all SMILES representations corresponded to their correct transfection values, assuming the experimental “source data” as the ground truth. This resulted in a curated dataset, which we make publicly available to enable direct comparison with the dataset originally used to fine-tune AGILE.

ii) Duplicate Entries Due to Geometric Isomerism: We identified 100 duplicate SMILES entries arising from the assignment of identical SMILES representations to cis and trans isomers, despite their distinct experimental transfection measurements. In the lipid library proposed by Xu et al. [26], some reactions yield cis-trans mixtures, while others exclusively produce trans isomers. Although the difference lies solely in geometric isomerism, their transfection efficiencies vary significantly. For example, lipid A17B4C5, which exists as a cis-trans mixture, has an experimental transfection value of 0.85, whereas A17B5C5, which has the same molecular formula but a pure trans structure, has a transfection efficiency of 1.54. This confirms that geometric isomerism has a substantial effect on transfection efficiency.

¹<https://www.nature.com/articles/s41467-024-50619-z#Sec41>

²<https://github.com/bowang-lab/AGILE>

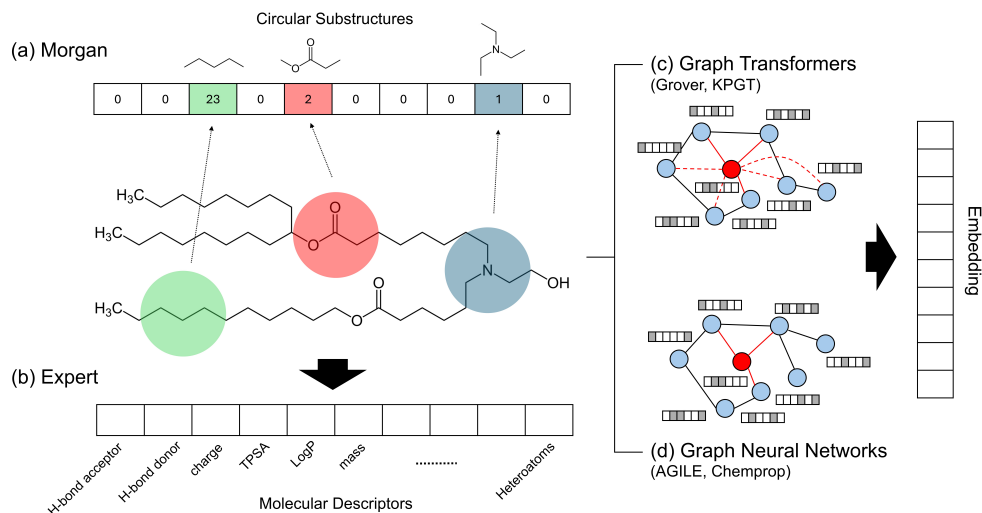


Figure 1: **Overview of molecular representation techniques.** (a) **Morgan fingerprints** encode molecular structures as binary vectors based on circular substructures. (b) **Expert descriptors** use predefined molecular properties, such as hydrogen bonding capacity, charge, and mass. (c) **Graph transformers** (e.g., Grover, KPGT) capture structural relationships through self-attention mechanisms, generating molecular embeddings. (d) **Graph neural networks (GNNs)** (e.g., AGILE, Chemprop) learn molecular representations by aggregating information from neighboring nodes in a molecular graph. The resulting embeddings from (c) and (d) can be used for downstream predictive modeling tasks.

However, AGILE did not account for this distinction, treating cis and trans isomers as the same molecule by assigning them identical SMILES representations. This misrepresentation results in two key issues: a) Chemically incorrect labeling – Cis and trans isomers are distinct molecules with different properties. b) Computational misrepresentation – The model encounters duplicate SMILES representations with conflicting transfection values, leading to inconsistencies and degraded predictive performance. Although the number of duplicates was relatively small compared to the overall dataset size, their presence introduced ambiguity and inconsistency in the dataset.

To resolve this issue, we removed the duplicate entries and retained only the trans isomers, resulting in a refined dataset comprising of 1,100 unique lipid molecules. The impact of these corrections on model performance is presented in Supplementary Figure S1, where we compare results before and after dataset refinement. Unless otherwise specified, this refined dataset was used for the training and evaluation of AGILE and all subsequent models in this study.

2.3 Impact of Feature Representations on LNP Transfection Prediction

Feature representation has a significant effect on model performance. An ideal representation must be both expressive and concise. Insufficient structural or chemical detail limits the model’s ability to learn relevant structure-property relationships, while overly complex feature spaces can impair model training and reduce generalizability. To systematically investigate how molecular representation impacts predictive accuracy, we evaluated three distinct feature sets for the representation of each ionizable lipid: count-based Morgan fingerprints, Expert RDKit-derived molecular descriptors, and Grover embeddings, a graph-based representation leveraging transformers.

Morgan fingerprints encode molecular substructures as bit vectors by algorithmically fragmenting molecules into atomic neighborhoods and expanding circular substructures around each atom [29]. In contrast, Expert molecular descriptors capture predefined physicochemical and topological properties, such as molecular weight, logP, and topological polar surface area (TPSA) [30, 31]. Graph-based representations, such as Grover embeddings, employ self-supervised learning on large molecular datasets to extract features directly from molecular graphs [23].

Additionally, end-to-end learned representations, as used in AGILE [26], integrate feature extraction within the predictive pipeline. While both AGILE and Grover are graph neural networks (GNNs), they differ in how they encode molecular structure. AGILE refines molecular representations through iterative neighborhood aggregation (graph isomorphism network), whereas Grover models long-range dependencies using self-attention. Figure 1 schematically illustrates these representation types.

To assess the structural distinctions among the three feature sets, we employed t-distributed stochastic neighbor embedding (t-SNE), a non-linear dimensionality reduction technique that preserves local relationships in high-dimensional

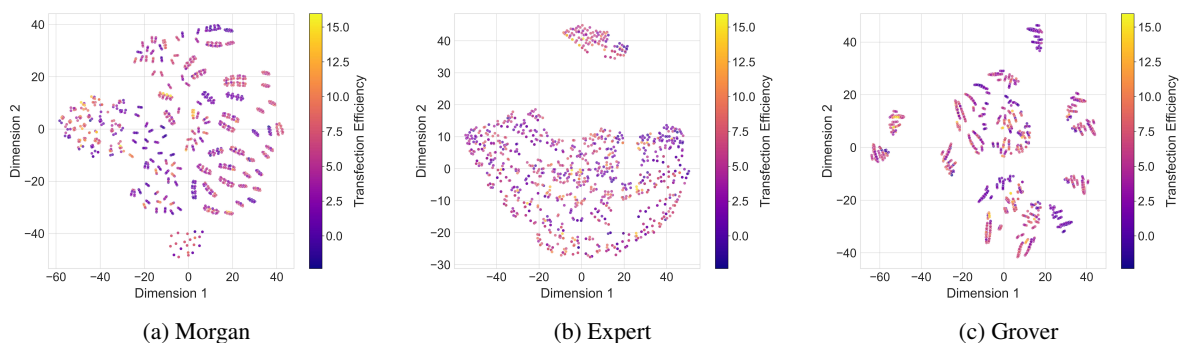


Figure 2: **t-SNE visualization of feature representations.** Each plot illustrates the distribution of LNP representations in a two-dimensional space, colored by transfection efficiency values. (a) **Morgan fingerprints** form well-defined clusters, suggesting they effectively capture key molecular substructures, leading to superior predictive performance. (b) **Expert descriptors** exhibit a more continuous spread, making them less discriminative but still informative. (c) **Grover embeddings** display a fragmented pattern, indicating less alignment with molecular properties relevant to transfection efficiency, which explains their weaker performance.

Method	Feature Set				Metrics			
	Morgan	Expert	Grover	End-to-End	R ²	RMSE	MAE	r
MLP	✓	✗	✗	✗	<u>0.7974</u>	<u>1.5018</u>	<u>1.1507</u>	<u>0.8959</u>
	✗	✓	✗	✗	0.5815	2.1585	1.6922	0.7639
	✗	✗	✓	✗	0.5171	2.3187	1.8576	0.7215
	✓	✓	✗	✗	0.8161	1.4308	1.1003	0.9053
	✓	✗	✓	✗	0.7489	1.6721	1.2311	0.8734
	✗	✓	✓	✗	0.5403	2.2622	1.7785	0.7398
	✓	✓	✓	✗	0.7449	1.6853	1.2162	0.8674
SVR	✓	✗	✗	✗	<u>0.7109</u>	<u>1.7942</u>	<u>1.4162</u>	<u>0.8615</u>
	✗	✓	✗	✗	0.5441	2.2529	1.7811	0.7446
	✗	✗	✓	✗	0.5236	2.303	1.8658	0.7287
	✓	✓	✗	✗	0.7285	1.7387	1.3739	0.8702
	✓	✗	✓	✗	0.6602	1.945	1.5216	0.827
	✗	✓	✓	✗	0.528	2.2925	1.8631	0.7325
	✓	✓	✓	✗	0.6593	1.9478	1.5254	0.8261
AGILE	✗	✗	✗	✓	0.2655	2.86	2.3328	0.5488
	✓	✗	✗	✓	0.706	1.8091	1.3497	0.8412
	✗	✓	✗	✓	0.2965	2.7987	2.2763	0.5618
	✗	✗	✓	✓	0.292	2.8076	2.2721	0.5765
	✓	✓	✗	✓	0.5676	2.1941	1.6587	0.7548
	✓	✗	✓	✓	<u>0.6705</u>	<u>1.9155</u>	<u>1.4274</u>	<u>0.8203</u>
	✗	✓	✓	✓	0.3355	2.7199	2.1461	0.5903
✓	✓	✓	✓	0.5271	2.2945	1.7435	0.7344	

Table 1: **Feature representation comparison across different models.** The table compares the performance of models across various feature sets, including Morgan fingerprints, expert-derived descriptors, Grover embeddings, and end-to-end learned representations. **Bold** highlight the best performance, and underlined denote the second-best. Overall, Morgan fingerprints consistently achieve the best predictive performance across models. Additionally, AGILE without the inclusion of our added features performs worse than all other models, highlighting the significance of feature representation in transfection efficiency prediction.

data (Figure 2) [32]. As seen in the figure, Morgan fingerprints exhibit distinct clustering, suggesting they effectively capture molecular substructures relevant to transfection efficiency. Expert descriptors display a more continuous spread, providing useful physicochemical insights but remaining less discriminative than Morgan fingerprints. Grover embeddings form fragmented clusters, indicating weaker alignment with molecular properties associated with transfection efficiency. Based on this clustering behavior, we expect Morgan fingerprints to serve as a stronger molecular representation for transfection efficiency prediction.

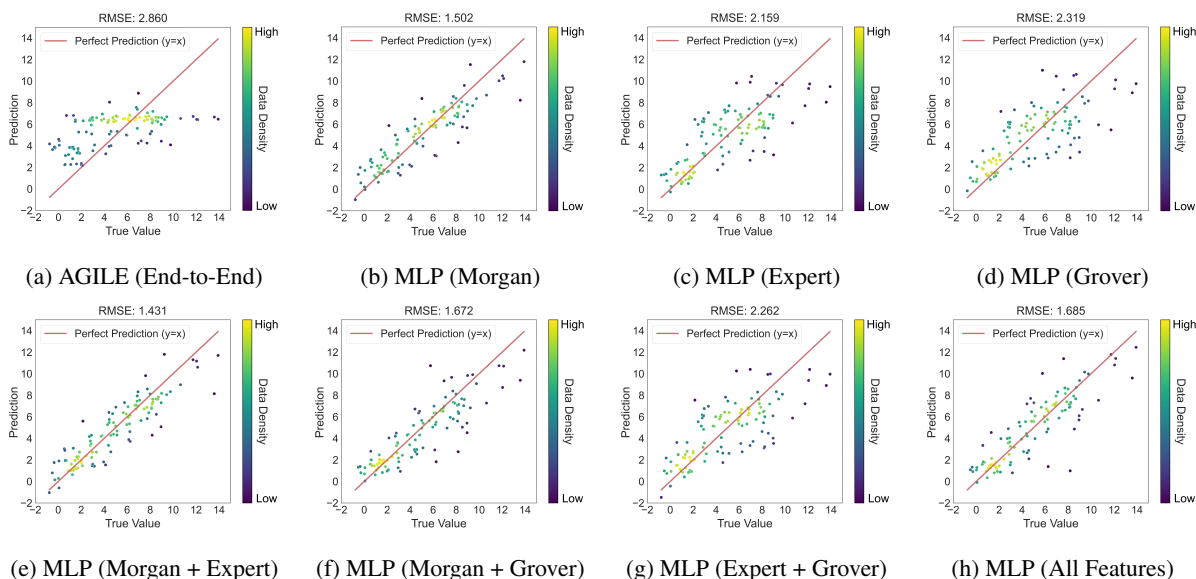


Figure 3: **Prediction vs. true value plots for different feature sets.** (a) AGILE model using end-to-end features. (b–h) MLP model trained with different feature sets, including Morgan, Expert, and Grover representations individually and in combination. *Morgan fingerprints* combined with *Expert descriptors* achieve the best performance with the lowest RMSE, demonstrating the advantage of combining domain-specific features with substructure-based Morgan fingerprints.

To quantify the predictive power of each feature set, we evaluated multiple models in LANTERN trained on individual and combined feature representations. We focused on: i) Multi-Layer Perceptron (MLP) – A deep learning model effective in capturing complex relationships. ii) Support Vector Regression (SVR) [33] – A robust traditional ML model leveraging kernel functions [34] for non-linear modeling. iii) AGILE (benchmark model) – A state-of-the-art (SOTA) graph-based model specifically designed for this dataset. All models were evaluated using the refined dataset to ensure fair comparisons. We applied a random data split and assessed model performance on the test set, maintaining a consistent evaluation framework.

Table 1 summarizes the results of this section. As seen, Morgan fingerprints consistently achieved the highest predictive performance across all models. Combining Morgan fingerprints with Expert descriptors further improved accuracy in MLP (Figure 3) and SVR (Supplementary Figure S2). On the other hand, graph-based representations (Grover embeddings and AGILE end-to-end embeddings) underperformed, emphasizing the limitations of data-driven feature extraction without explicit molecular substructure encoding. In this context, AGILE’s predictive performance remains limited despite using a molecular descriptor computed using the Mordred toolbox [35] to refine lipid representations within the pre-trained graph encoder. We also extended AGILE by incorporating additional explicit molecular features and evaluated their effect on model accuracy (Supplementary Figure S3). Notably, the inclusion of Morgan fingerprints led to a substantial improvement in AGILE’s predictive accuracy (Table 1), further underscoring the value of chemically meaningful descriptors for LNP transfection prediction. It should be noted that Grover’s pretraining data primarily consists of small molecules [23], which may limit the relevance of its learned representations when applied to structurally distinct and larger lipid molecules.

Our findings underscore the superior performance of Morgan fingerprints and their combinations with Expert descriptors across diverse ML models. While graph-based representations offer a promising data-driven alternative, their effectiveness remains limited in certain cases without explicit molecular substructure encoding. These insights provide valuable guidance for selecting molecular representations in future predictive modeling efforts.

2.4 Comparative Analysis of ML Models for LNP Transfection Prediction

After observing the superior performance of Morgan fingerprints combined with Expert descriptors in MLP, SVR, and even AGILE, we sought to address three key questions: (i) *Can this performance generalize to other ML models, and how do models using these feature sets compare to the state-of-the-art AGILE framework for LNP transfection prediction?* (ii) *Which ML model achieves the highest predictive performance when using Morgan fingerprints alone or in combination with Expert descriptors?* (iii) *How do other graph-based models, with their own end-to-end feature extraction strategies, perform relative to AGILE and models utilizing explicit molecular substructure encoding?*

Method	Feature Set			Metrics			
	Morgan	Expert	End-to-End	R ²	RMSE	MAE	r
MLP	✓	✗	✗	0.7974	1.5018	1.1507	0.8959
	✓	✓	✗	0.8161	1.4308	1.1003	0.9053
Transformer	✓	✗	✗	0.6555	1.9585	1.5181	0.81
	✓	✓	✗	0.6368	2.011	1.5381	0.8005
SVR	✓	✗	✗	0.7109	1.7942	1.4162	0.8615
	✓	✓	✗	0.7285	1.7387	1.3739	0.8702
RF	✓	✗	✗	0.6976	1.835	1.3548	0.84
	✓	✓	✗	0.7169	1.7753	1.3391	0.848
kNN	✓	✗	✗	0.6001	2.11	1.6109	0.7769
	✓	✓	✗	0.6148	2.071	1.5969	0.7866
KPGT	✗	✗	✓	0.6655	1.9298	1.4597	0.8211
Chemprop	✗	✗	✓	0.5215	2.3081	1.7908	0.7248
AGILE	✗	✗	✓	0.2655	2.86	2.3328	0.5488

Table 2: **Performance comparison across models and feature sets.** The table presents the predictive performance of various ML models in LANTERN trained with different feature representations, including Morgan fingerprints, expert descriptors, and end-to-end learned embeddings, compared against the AGILE baseline. MLP consistently achieves the best performance, with its highest accuracy observed when using the Morgan fingerprints and expert descriptors combination, as indicated by the **bold** values. Underlined values represent the second-best performance.

To answer these questions, we systematically evaluated the predictive performance of diverse ML architectures in LANTERN, encompassing traditional ML, feedforward, and graph-based deep learning models, applying multiple evaluation strategies to ensure robust benchmarking. Specifically, we assessed five representative models: multi-layer perceptron (MLP), transformer-based models, support vector regression (SVR), random forest (RF), and k-nearest neighbors (kNN), using Morgan and Expert descriptors individually or in combination. MLP and transformer-based models were selected to represent feedforward architectures. MLP has demonstrated strong predictive capabilities across various domains by efficiently capturing complex feature interactions. While transformers [36] have not been widely explored for molecular modeling, their self-attention mechanism [37] enables them to capture complex interactions, making them a promising architecture to investigate. Among traditional ML models, we included SVR, RF, and kNN, which have demonstrated robust predictive performance in molecular learning tasks. The key distinction between these models lies in their learning strategies: SVR and RF are trainable models, with SVR leveraging kernel-based flexibility to capture nonlinear dependencies, while RF [38] utilizes ensemble learning to reduce variance. In contrast, kNN [39] is a non-parametric algorithm that estimates target values based on local feature similarities, without requiring explicit model training.

Additionally, we benchmarked these models against the AGILE framework [26] and included Chemprop [40], a graph neural network (GNN) model similar to AGILE that directly processes molecular graphs to extract structural features. This inclusion enables a broader evaluation of GNN-based approaches in LNP transfection prediction. While Chemprop has been widely applied in molecular property prediction, AGILE is specifically designed for LNP transfection prediction and represents the domain-specific state-of-the-art model. We also evaluated KPGT (Knowledge-Powered Graph Transformer) [41], which differs from conventional GNNs by incorporating transformer-based self-attention mechanisms to capture higher-order structural dependencies in molecular graphs. All these graph-based models rely on end-to-end feature extraction, dynamically learning molecular representations during pretraining and training, with feature generation fully integrated into the predictive pipeline.

All models were evaluated on the refined dataset to ensure fair comparisons. We employed the same random data split as in previous sections and assessed model performance on the test set, ensuring a consistent evaluation framework. Table 2 summarizes key regression metrics for all models, and Figure 4 presents prediction vs. true value plots using the optimal feature representations for each model. Among all tested models, MLP achieved the highest accuracy when using Morgan fingerprints combined with Expert descriptors, reinforcing its capability to model complex molecular relationships effectively. Traditional ML models, such as SVR and RF, also performed competitively, highlighting their suitability for molecular property prediction when coupled with Morgan and Expert descriptors. Notably, even kNN outperformed AGILE, suggesting the robustness of explicitly encoded molecular substructure features for LNP transfection prediction.

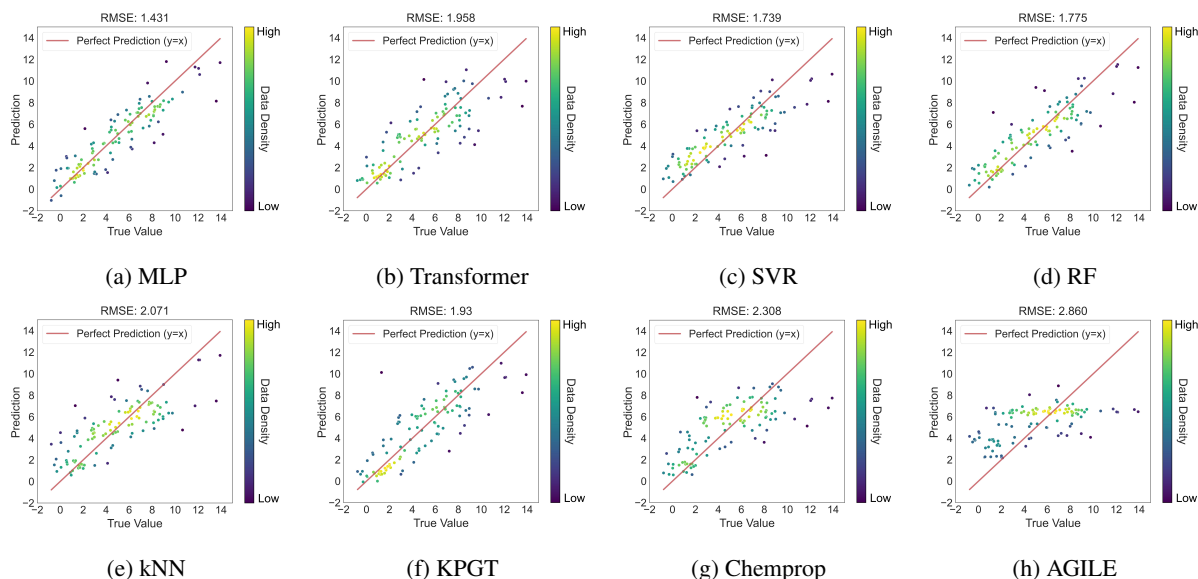


Figure 4: **Prediction vs. true value plots for different models.** Each model is evaluated using its optimal feature representation, as determined by previous analyses. (a–h) show the predictive performance of MLP, Transformer, SVR, RF, kNN, KPGT, Chemprop, and AGILE, respectively. MLP achieves the highest accuracy among all models, highlighting its strong capacity for capturing complex relationships in the data. Traditional ML models such as SVR and RF perform competitively, while graph models like AGILE and Chemprop exhibit lower predictive accuracy.

While AGILE exhibited the worst performance among all tested models, the other two graph-based approaches—Chemprop and KPGT—demonstrated notably better predictive accuracy, suggesting that data-driven feature extraction can be effective for LNP transfection prediction when implemented using proper architectures and training strategies. This observation further underscores the limitations of AGILE, which may stem from suboptimal choices in its training and pretraining methodologies. Among the graph-based architectures evaluated, KPGT achieved the highest predictive accuracy; however, its performance remained inferior to the top-performing models that utilized explicit molecular substructure encoding, namely MLP, SVR, and RF. This relative underperformance is likely attributable to the model’s limited capacity to fully capture key molecular features relevant to transfection efficiency when trained on a small, domain-specific dataset. These findings suggest that graph-based models may require either larger training datasets or pretraining on lipid-rich molecular corpora to effectively learn meaningful representations and enhance their performance in the context of LNP transfection prediction. Given the limited availability of high-quality labeled data, simpler deep learning architectures and traditional ML models combined with well-selected representations may serve as more effective alternatives, at least until larger, well-curated datasets become consistently available in the field.

Additionally, ML models using explicit feature representations are computationally more efficient, requiring less training time and fewer resources compared to graph-based architectures. Among these approaches, MLP demonstrated the strongest performance, likely due to its ability to capture nonlinear relationships and complex interactions more effectively than traditional ML models, which rely on handcrafted features or tree-based decision processes.

Overall, these results highlight the effectiveness of ML models leveraging explicit molecular representation for accurate prediction of transfection efficiency. In contrast, the limitations observed in graph-based models underscore the need for enhanced model architectures or hybrid approaches that integrate domain-specific molecular features with graph-based learning. Additionally, the performance of graph-based models may benefit from access to larger, lipid-relevant pretraining and fine-tuning datasets, enabling the models to learn more chemically meaningful and task-relevant embeddings for LNP transfection prediction.

2.5 Impact of Murcko Scaffold Splitting on Model Performance

To assess the generalization capabilities of LANTERN models under a more stringent data partitioning scheme, we use Murcko scaffold splitting to generate distinct training, validation, and test sets. This strategy, employed in the AGILE framework, groups molecules based on their core scaffolds, ensuring that structurally distinct compounds appear in the training, validation, and test sets. This approach provides a more realistic evaluation of model performance when applied to unseen chemical structures, which is crucial in drug discovery and molecular property prediction. However,

Method	Feature Set			Metrics			
	Morgan	Expert	End-to-End	R ²	RMSE	MAE	r
MLP	✓	✗	✗	0.5265	1.9305	1.5465	0.7337
	✓	✓	✗	0.4532	2.0746	1.7726	0.7344
Transformer	✓	✗	✗	0.3324	2.2924	1.8597	0.6552
	✓	✓	✗	0.4097	2.1555	1.7421	0.6621
SVR	✓	✗	✗	0.3082	2.3336	2.0003	0.6374
	✓	✓	✗	0.3157	2.3209	1.9835	0.6425
RF	✓	✗	✗	0.3496	2.2627	1.7943	0.6043
	✓	✓	✗	0.4747	2.0334	1.5947	0.6895
kNN	✓	✗	✗	0.6146	1.7419	1.3644	0.7955
	✓	✓	✗	<u>0.5919</u>	<u>1.7923</u>	<u>1.4177</u>	<u>0.7892</u>
KPGT	✗	✗	✓	0.4878	2.0079	1.5751	0.7173
Chemprop	✗	✗	✓	0.5129	1.9582	1.4912	0.7188
AGILE	✗	✗	✓	0.0057	2.7976	2.3389	0.4690

Table 3: **Performance comparison across models and feature sets under Murcko scaffold split.** This table presents the predictive performance of various ML models trained with different feature representations, including Morgan fingerprints, expert descriptors, and end-to-end learned embeddings. **Bold** highlight the best performance, and underlined denote the second-best. Due to the more challenging scaffold-based data split, overall performance is lower compared to random splitting. While most models show a decline in accuracy, kNN and Chemprop maintain similar performance levels, suggesting their robustness to distribution shifts. kNN achieves the best performance, followed by MLP, while AGILE exhibits the lowest predictive accuracy.

in cases where the dataset is relatively small, scaffold-based splitting can lead to excessive data fragmentation, reducing the amount of structurally similar training examples available for learning and making the task more challenging.

The predictive performance of all models under Murcko scaffold splitting is summarized in Table 3, with prediction vs. true value plots presented in Supplementary Figure S4. Compared to the random split case, most models exhibit a decline in accuracy in LNP transfection prediction, highlighting the increased difficulty of generalizing to unseen molecular scaffolds. Notably, kNN and Chemprop maintain similar predictive performance, indicating their robustness to distribution shifts. In contrast, other models experience a noticeable drop in accuracy, suggesting their reliance on learned patterns that may not generalize well to novel scaffolds, particularly in the context of small datasets.

Despite this challenge, kNN emerges as the top-performing model in the scaffold-based setting, followed closely by MLP, which previously demonstrated superior performance in the random split scenario. This suggests that nonparametric methods like kNN may be less sensitive to scaffold-based domain shifts, while deep learning models such as MLP, despite their higher capacity, require more structurally diverse training data to generalize effectively. AGILE, which was originally designed using this splitting strategy, continues to show the lowest predictive accuracy, reinforcing the observation that it struggles to extract meaningful representations in low-data regimes without extensive pretraining.

These results demonstrate the significant impact of data-splitting strategies on model performance. Overall, all models outperformed AGILE, even when evaluated using the more stringent Murcko scaffold splitting strategy. It is important to note that while Murcko scaffold splitting provides a rigorous assessment of a model’s generalization ability by enforcing structural dissimilarity between training and test sets, its applicability to small datasets is limited. In such cases, this approach may artificially exaggerate performance differences between models by creating non-overlapping chemical spaces, which do not necessarily reflect realistic generalization scenarios encountered in practical applications.

2.6 Error Distribution and Ranking-Based Evaluation of Regression Models

To further assess model performance, we analyzed the distribution of relative errors and evaluated LANTERN models based on ranking accuracy. These analyses provide complementary insights into the reliability of LNP transfection prediction beyond standard regression metrics.

The relative error histograms provide valuable insights into the stability and robustness of model predictions, complementing regression metrics such as RMSE and R² presented in Table 2. It is important to note that relative error distributions do not always align directly with standard regression metrics and can reveal additional nuances related to model uncertainty. Relative error is defined as the absolute difference between the predicted and true transfection

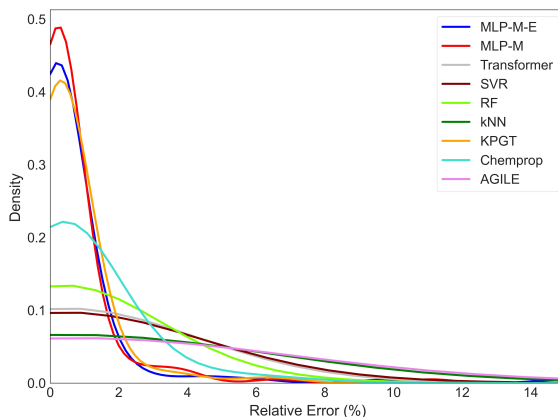


Figure 5: **Relative error distribution across different models.** This figure presents the relative error histograms for nine models evaluated, including two MLP variants trained with Morgan fingerprints (MLP-M) and Morgan fingerprints combined with expert descriptors (MLP-M-E). For models utilizing multiple feature sets, the best-performing configuration is selected based on predictive accuracy. The distribution of errors highlights the reliability and precision of each model, with narrower and more concentrated histograms indicating superior predictive performance.

efficiency, normalized by the true value. Lower relative error values indicate higher predictive accuracy. In terms of error distribution, narrower and more concentrated distributions reflect greater reliability and reduced variability in predictions, whereas broader distributions suggest increased uncertainty and diminished predictive consistency.

Figure 5 presents the relative error distributions for all models, evaluated on the test set under random splitting. Our results indicate that MLP not only consistently achieves the highest accuracy across regression analyses (as shown in Table 2) but also exhibits a more concentrated error distribution, suggesting stable performance with fewer extreme mispredictions. Despite higher regression error, KPGT maintains a relative error distribution comparable to MLP, indicating robustness and reduced variability in predictions. Chemprop shows a slightly wider relative error distribution, which, combined with its higher regression error, makes it inferior to MLP and KPGT but still superior to other models.

In contrast, transformer-based and traditional ML models (SVR, RF, kNN) display broader tails in their error distributions, reflecting greater variability in predictions. Among all models, AGILE exhibits the widest relative error distribution, further reinforcing its poor predictive performance and lack of reliability in transfection efficiency estimation. These discrepancies underscore the importance of evaluating models using multiple criteria.

Instead of presenting exact numerical values and regression metrics for LNP transfection efficiency, Xu et al. [26] employed a ranking-based evaluation, categorizing predictions into percentile bins to assess the predictive performance of AGILE. This approach utilizes confusion matrices to illustrate how effectively the model rank transfection efficiency values into discrete percentile groups. We applied this visualization method to various models trained using random splitting (Figure 6). In these matrices, diagonal elements represent correctly ranked predictions, while off-diagonal elements indicate misclassified rankings.

The results suggest that MLP achieves the highest ranking accuracy, with the largest proportion of correctly classified percentile bins along the diagonal. The average ranking accuracy across all bins for MLP is 50.0%, with particularly strong performance in predicting high transfection formulations (73.7%) and low transfection formulations (57.9%). In contrast, AGILE continues to exhibit the weakest performance, with an average accuracy of 22.7%, correctly identifying only 26.3% of high transfection formulations and 47.4% of low transfection formulations, further highlighting its limitations in transfection efficiency prediction.

Among graph-based and traditional models, KPGT and RF demonstrate comparable accuracy to MLP, with KPGT excelling at identifying very high and very low transfection formulations, while RF maintains a more uniform accuracy across the bins. Overall, these findings reinforce the superior generalization capability of MLP models, both in terms of direct regression accuracy and ranking-based evaluation, for this specific task and dataset.

3 Discussion

The present study systematically evaluates the predictive performance of various machine learning (ML) models for lipid nanoparticle (LNP) transfection efficiency prediction, emphasizing the importance of feature selection, model

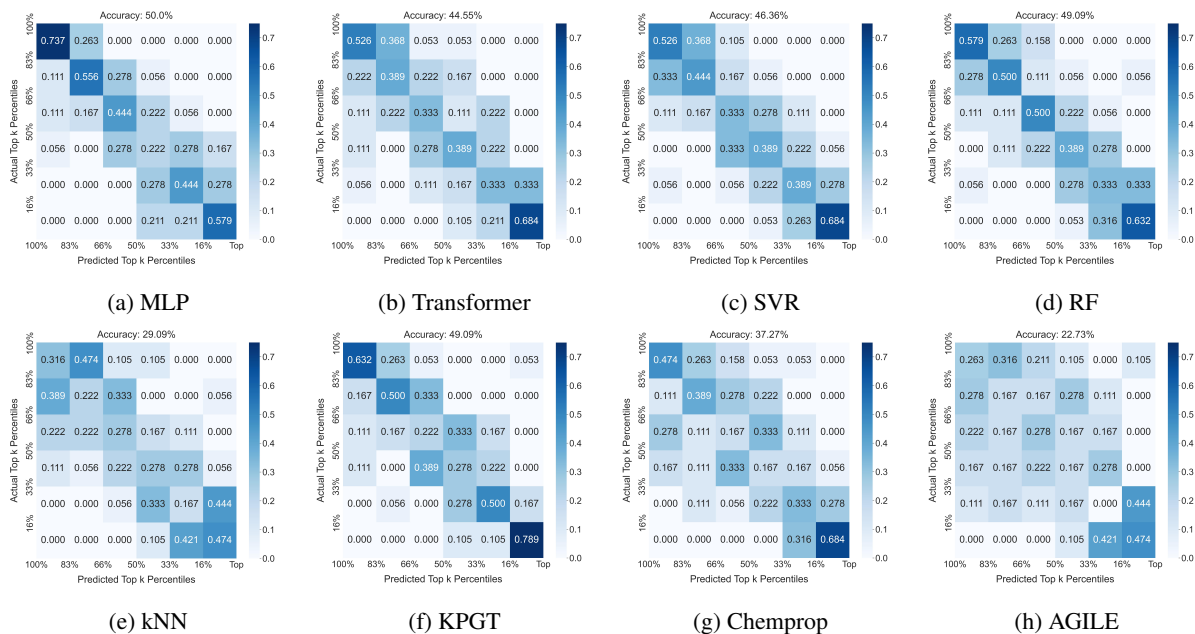


Figure 6: **Confusion matrices for different models using the AGILE ranking-based evaluation approach.** Each matrix represents the performance of a model on the test set, where the best-performing feature set is selected for each model. The confusion matrices are constructed based on percentile-based ranking, where true and predicted transfection efficiencies are assigned to discrete percentile bins. The diagonal elements indicate correct rankings, while off-diagonal elements reflect ranking misclassifications. Higher values along the diagonal correspond to better performance. MLP achieves the highest ranking accuracy, while AGILE shows the lowest predictive ranking performance.

architecture, and evaluation strategies. We used the AI-Guided Ionizable Lipid Engineering (AGILE) platform, developed by Xu et al. [26], as a benchmark. AGILE integrates a graph neural network (GNN) encoder derived from the MolCLR model [27], pre-trained on 60,000 virtual lipid structures, with combinatorial chemistry and is considered the state-of-the-art regression model for predicting LNP transfection efficiency. AGILE was fine-tuned using transfection efficiency data from HeLa cells for a library of 1,200 ionizable lipids, and its predictive performance was evaluated using a ranking-based approach, wherein both predicted and experimental transfection values were categorized into percentile bins to assess the model’s ability to prioritize high- and low-performing lipid formulations.

A rigorous audit of this dataset revealed two significant issues: (i) 235 inconsistencies between experimental values and the dataset used for fine-tuning, which we manually corrected, and (ii) 100 duplicate SMILES assigned to cis-trans and trans isomers despite their distinct experimental transfection measurements. The latter issue was addressed by removing the duplicates and retaining only the trans isomers, ensuring structural uniqueness and consistency in biological activity labeling, in accordance with the approach outlined by Belenahalli Shekarappa et al. [42]. These errors, including incorrect labeling and duplicate SMILES representations with conflicting transfection values, degrade predictive performance and reduce model reliability. After dataset refinement, which resulted in a curated dataset of 1,100 unique molecules, AGILE’s accuracy improved marginally from 24.17% to 24.55% on the test set (Figure S1). This reported accuracy may appear to contradict the 28.83% accuracy reported by Xu et al. [26], but this discrepancy arises from their inclusion of training, validation, and test data in performance evaluation, which artificially inflates accuracy. Our evaluation was based strictly on test-set performance, ensuring a more rigorous assessment of generalization capability.

While AGILE is currently regarded as the state-of-the-art regression model for LNP transfection prediction, its predictive accuracy remains suboptimal. To develop a more robust framework, we systematically evaluated three distinct feature sets: Morgan fingerprints, Expert RDKit-derived molecular descriptors, and Grover embeddings, a graph-based representation leveraging transformers. These feature representations were used to train Multi-Layer Perceptron (MLP)—a deep learning model capable of capturing complex molecular relationships—and Support Vector Regression (SVR)—a traditional ML approach that employs kernel functions for nonlinear modeling. Their performance was then compared with AGILE, a GNN model specifically designed for this dataset. Our findings indicate that Morgan fingerprints, either alone or in combination with Expert descriptors, consistently yielded the highest predictive performance, highlighting the effectiveness of explicit molecular substructure encoding in LNP transfection prediction.

Morgan fingerprints encode molecular substructures as bit vectors by fragmenting molecules into atomic neighborhoods and iteratively expanding circular substructures around each atom [29]. These fingerprints are extensively utilized in molecular similarity-based tasks [43], including virtual screening of bioactive molecules against target proteins [44] and the development of structure-activity relationship models for diverse applications such as ADME-Tox prediction [45], bioactivity assessment of natural compounds for therapeutic potential [46], drug combination sensitivity and synergy prediction [47], and identification of novel inhibitors in protein-target screening [42]. Despite their ability to effectively capture substructural similarity patterns, Morgan fingerprints lack direct interpretability. The choice between similarity-based screening and ML-based predictions is inherently task-dependent, as highlighted by Tejera et al. [48], who demonstrated that while certain compound-cell line interactions are better predicted using similarity-based approaches, others benefit more from ML models.

In this study, we employed count-based Morgan fingerprints (C-MF), introduced by Zhong et al. [49], which incorporate substructure frequency for enhanced molecular representation. Binary Morgan fingerprints (B-MF) only encode the presence or absence of molecular substructures but do not capture their frequency. Zhong et al. [49] compared C-MF and B-MF across six ML algorithms (ridge regression [50], SVM [51], kNN, RF, XGBoost [52], and CatBoost [53]) on ten datasets related to water contaminants and demonstrated that C-MF outperforms B-MF in nine of ten datasets.

Morgan fingerprints, both alone and in combination with Expert descriptors, also led to superior predictive performance for other ML models, including transformers, RF, and kNN. Expert molecular descriptors encode predefined physico-chemical and topological properties, such as molecular weight, logP, and topological polar surface area (TPSA) [30, 31]. These descriptors integrate domain-specific knowledge, providing interpretable features that enhance the understanding of molecular properties critical to transfection efficiency. The improved predictive performance achieved by combining Morgan fingerprints with Expert descriptors aligns with previous studies suggesting that integrating Morgan fingerprints with other molecular representations enhances predictive accuracy and model robustness. Zhou et al. [54], for instance, demonstrated that incorporating Morgan fingerprints into the FINDSITE suite improved ligand homology modeling, traditional ligand similarity methods, and ML-based virtual screening approaches, highlighting the added value of explicit molecular substructure encoding in predictive tasks.

When comparing Morgan fingerprints to Expert descriptors, our findings indicate that Morgan fingerprints consistently outperformed Expert descriptors in predicting LNP transfection efficiency. However, this is not universally the case across all applications, as the effectiveness of molecular descriptors depends on the specific predictive task and dataset characteristics. For instance, Tayyebi et al. [55] showed that descriptor-based molecular representations generated using the Mordred package [56] resulted in better accuracy for aqueous solubility prediction compared to Morgan fingerprints when used with RF and multiple linear regression (MLR). Similarly, Seal et al. [57] demonstrated that Cell Painting descriptors outperformed both ErG fingerprints and Morgan fingerprints for cytotoxicity and proliferation assay predictions.

Our study also highlights the limitations of graph-based representations, such as Grover embeddings and AGILE's end-to-end learned embeddings, in LNP transfection prediction. Grover embeddings employ self-supervised learning and leverage graph-transformer architectures trained on large molecular datasets to extract structural features directly from molecular graphs [23]. However, this data-driven feature extraction approach limits interpretability, as it does not explicitly incorporate domain-specific chemical knowledge. Fang et al. [58] suggested that while GNNs and their variants can automatically learn molecular representations from molecular graphs, they often overlook critical chemical domain knowledge during feature extraction. They argued that simple molecular graphs alone are insufficient for robust molecular representation learning, as they fail to encode deep semantic features relevant to chemistry. Additionally, they noted that GNNs suffer from over-smoothing, a phenomenon that arises from the excessive propagation of information across long distances in the graph, ultimately leading to indistinguishable node representations.

To address limitations in conventional graph-based models, Fang et al. [58] proposed incorporating chemical domain knowledge through Morgan fingerprints, which effectively mitigates over-smoothing and reduces reliance on long-distance information propagation in molecular graphs. They demonstrated significant improvements in predicting various molecular properties, including toxicity and lipophilicity, underscoring the value of explicitly incorporating substructural chemical information into graph-based model architectures. This observation aligns with our results, which show that integrating Morgan fingerprints into AGILE substantially improved predictive performance of the model (Table 1). The enhanced accuracy is likely attributable to the injection of domain-specific chemical knowledge, resulting in more chemically meaningful representations than those derived from purely data-driven feature extraction alone. Interestingly, the incorporation of Expert descriptors into AGILE did not lead to significant improvement in predictive performance. This is notable because AGILE includes a molecular descriptor encoder that processes descriptors—computed using the Mordred toolbox [35]—to update the lipid structure representation in the pre-trained graph encoder. Our findings suggest that this integration strategy may not be effective for improving transfection prediction accuracy. A similar pattern was observed when Expert descriptors were combined with Grover embeddings

for training MLP and SVR (Table 1). In contrast to the improvements seen with Morgan fingerprints, the addition of Expert descriptors did not enhance predictive performance relative to models trained on Grover features alone. This further underscores the superior utility of Morgan fingerprints in providing chemically informative features for LNP transfection prediction, compared to generic physicochemical descriptors in this context.

Given AGILE's poor performance, we investigated whether this limitation stemmed from fundamental challenges in feature extraction from molecular graphs or was specific to AGILE's architecture. Li et al. [41] suggested that many self-supervised learning-based methods that use pre-trained GNNs to address data scarcity in molecular property prediction suffer from two key obstacles: (i) the lack of a well-defined self-supervised learning strategy and (ii) the limited capacity of GNNs to extract chemically meaningful representations. To explore this, we tested KPGT, a self-supervised graph transformer developed by Li et al. [41], which was designed to overcome these challenges and generate generalizable and robust molecular representations. We also evaluated Chemprop, a GNN-based model that integrates message-passing and aggregation functions to enhance molecular feature extraction. Our results indicate that KPGT demonstrated superior predictive performance compared to both AGILE and Chemprop, underscoring the critical role of pretraining strategies and model architecture in the success of graph-based molecular property prediction. The KPGT framework incorporates a backbone model, known as the Line Graph Transformer (LiGhT), which has been pre-trained on approximately two million molecules from the ChEMBL29 dataset [59] as part of its knowledge-guided pretraining strategy. Through extensive computational validation across 63 molecular property prediction datasets, KPGT has been shown to outperform traditional GNN-based approaches, further reinforcing the importance of advanced pretraining strategies in molecular ML tasks [41].

Our findings indicate that MLP consistently outperforms all other models across multiple evaluation criteria, including regression accuracy, relative error distribution, and ranking-based assessments. While GNNs have shown promise in other molecular property prediction tasks, their reliance on large datasets and extensive pretraining makes them less effective for small datasets, such as those used for LNP transfection prediction. Our results suggest that simpler ML models, particularly MLP, provide more reliable predictions when well-engineered molecular representations such as Morgan fingerprints are used. This aligns with prior studies emphasizing the importance of domain-specific feature engineering in enhancing predictive accuracy [58].

By demonstrating the effectiveness of MLP combined with Morgan fingerprints and Expert descriptors, we establish a computationally efficient framework for LNP transfection prediction. This has significant implications for experimental design, virtual screening, and the prioritization of lipid structures for formulation in nanomedicine. Additionally, the refined dataset and benchmarking pipeline offer an improved alternative to AGILE, facilitating the development of more accurate predictive tools for lipid-based therapeutics.

The provided framework and the proposed models offer several advantages over AGILE. While AGILE primarily employs ranking-based evaluation to assess the model's ability to prioritize molecules based on transfection efficiency, our study extends the comparison by evaluating different models using regression-based evaluation metrics, which provide more quantitative and informative insights. To ensure an equivalent comparison, we also conducted ranking-based evaluations for all tested models alongside AGILE. In the study by Xu et al. [26], AGILE's performance was originally assessed using confusion matrices computed across the entire dataset (i.e., including training, validation, and test splits), which artificially inflates accuracy by incorporating training data. Under these conditions, AGILE achieved 41% accuracy in predicting high-transfection formulations (83rd–100th percentile) and low-transfection formulations (0th–16th percentile) (Figure S1). However, when we evaluated AGILE solely on the test split, these accuracies dropped to 40% for low-transfection formulations and 20% for high-transfection formulations, highlighting its poor generalization ability.

All tested models outperformed AGILE in terms of ranking-based accuracy for both high and low transfection efficiency ranges, as well as in overall ranking accuracy, when evaluated strictly on the test set (Figure 6). Specifically, the prediction accuracy for low-transfection and high-transfection formulations was 57.9% (low) and 73.7% (high) for MLP, 57.9% (low) and 73.7% (high) for SVR, and 78.9% (low) and 63.2% (high) for KPGT. These findings highlight AGILE's weak performance compared to deep learning models (e.g., MLP) and traditional ML approaches (e.g., SVR) that leverage explicit molecular features, as well as graph-based models (e.g., KPGT) that employ optimized end-to-end feature extraction.

Furthermore, these findings underscore the inadequate selection of benchmark models used in the evaluation of AGILE, as presented by Xu et al. [26]. The models chosen for benchmarking during AGILE's development exhibit poor performance, are not competitive by current standards, and do not adequately represent state-of-the-art methodologies in molecular property prediction. For instance, AGILE was benchmarked against Ridge regression, which yielded an R^2 of -1.036 and a Pearson correlation of 0.514 , values markedly inferior to those obtained by the models evaluated in this study. A more appropriate and meaningful comparison would involve models capable of learning complex, non-linear relationships from molecular structure, such as multi-layer perceptrons (MLPs) and transformer-based graph

architectures. These models are more aligned with the complexity and learning capacity of AGILE. Therefore, the benchmarking strategy employed in the original AGILE study likely overstated the model’s relative performance by failing to include more competitive and representative baseline models.

Despite the improvements achieved in this study, certain limitations remain. The dataset, while refined, is still relatively small, which limits the generalizability of deep learning approaches. Future research should explore the integration of external datasets, domain-adapted transfer learning strategies, and experimental validation of high-confidence predictions to bridge the gap between computational modeling and real-world applications. Overall, our findings underscore the advantages of feature-driven ML models over purely end-to-end approaches for LNP transfection prediction, particularly in small dataset scenarios.

4 Methods

4.1 ML Models and Training Procedure

We evaluated five ML models that have been widely applied across domains [60, 61], including multi-layer perceptron (MLP), transformer [36], support vector regression (SVR) [33], random forest (RF) [38], and k-nearest neighbors (kNN) [39]. These models were selected due to their strong performance in regression tasks and their diversity in learning paradigms. In addition, we benchmarked three domain-specific models developed for molecular property prediction: Chemprop, KPGT, and AGILE. All model hyperparameters were tuned to ensure optimal performance, except for AGILE, which was used directly from the original implementation without any modifications. All models were trained using a curated dataset derived from HeLa cell transfection experimental data originally reported by Xu et al. [26]. The final dataset was rigorously validated to ensure consistency with the original experimental measurements and to eliminate redundancy by removing duplicate SMILES representations associated with geometric isomers, thereby preserving structural uniqueness and ensuring data integrity.

For the MLP, we used a seven-layer feedforward architecture (including the output layer) with hidden layer sizes of 200, 300, 500, 500, 300, and 200, each followed by ReLU activation. The model was trained for up to 100 epochs using the Adam optimizer [62] with a learning rate of 0.0002. Mean squared error (MSE) was used as the loss function, and early stopping was applied to prevent overfitting.

The transformer model was implemented using an encoder-based architecture with five layers, each containing two attention heads. The hidden dimension within each feedforward layer was set to 500, and the model dimension (embedding size) was set to 100. It was trained for 100 epochs using the Adam optimizer with a learning rate of 0.0002, MSE loss, and early stopping.

For traditional models, the SVR model uses a radial basis function (RBF) kernel to capture complex nonlinear relationships in the data. This kernel was selected due to its strong ability to approximate highly nonlinear mappings between input features and target values, making it a powerful choice for small to medium-sized datasets where flexible function fitting is beneficial. The RF model was configured with 100 estimators and used the squared error criterion. For kNN, we set the number of neighbors to 5 and used uniform weighting with mean aggregation.

For domain-specific models, we used the official AGILE implementation with the same training settings reported in the original study [26]. For Chemprop, we trained the graph encoder and regressor on our curated dataset using MSE loss for 100 epochs, with a hidden dimension of 500 in the regressor. For KPGT, we used their pretrained model embeddings and trained a three-layer regressor with a hidden dimension of 512 for 20 epochs.

4.2 Feature Representations

We employed three types of molecular features: Morgan fingerprints, Expert descriptors, and Grover embeddings. Morgan fingerprints were computed using the DeepChem [63] Python library, generating 2048-dimensional count-based circular fingerprints. Expert descriptors were extracted using RDKit’s [30] 210-dimensional built-in descriptor module. For Grover embeddings [23], we used the pretrained model provided by the original authors, applying the default configuration.

4.3 Evaluation Metrics

Model performance was evaluated using four standard regression metrics: coefficient of determination (R^2), root mean squared error (RMSE), mean absolute error (MAE), and Pearson correlation coefficient (r).

- **R²**: Measures the proportion of variance in the target explained by the model. Higher values indicate better performance. It is computed as:

$$R^2 = 1 - \frac{\sum_{i=1}^n (y_i - \hat{y}_i)^2}{\sum_{i=1}^n (y_i - \bar{y})^2} \quad (1)$$

where \hat{y}_i is the predicted value, y_i is the true value, and \bar{y} is the mean of the observed data.

- **RMSE**: Quantifies the average squared difference between predicted and true values. Lower values indicate better accuracy and are sensitive to outliers. It is calculated as:

$$\text{RMSE} = \sqrt{\frac{1}{n} \sum_{i=1}^n (\hat{y}_i - y_i)^2} \quad (2)$$

- **MAE**: Measures the average magnitude of prediction errors. Unlike RMSE, it treats all errors equally. It is defined as:

$$\text{MAE} = \frac{1}{n} \sum_{i=1}^n |\hat{y}_i - y_i| \quad (3)$$

- **Pearson correlation (r)**: Captures the linear correlation between predictions and ground truth, ranging from -1 (perfect inverse) to 1 (perfect direct correlation):

$$r = \frac{\sum_{i=1}^n (\hat{y}_i - \bar{\hat{y}})(y_i - \bar{y})}{\sqrt{\sum_{i=1}^n (\hat{y}_i - \bar{\hat{y}})^2} \cdot \sqrt{\sum_{i=1}^n (y_i - \bar{y})^2}} \quad (4)$$

We additionally computed the relative error for each sample as:

$$\text{Relative Error} = \frac{|\hat{y} - y|}{y} \quad (5)$$

where \hat{y} is the predicted value and y is the ground truth. Relative error distributions were used to assess model uncertainty and stability.

To complement regression analysis, we adopted the percentile-based classification approach used in the AGILE framework. Ground truth and predicted transfection values were mapped to percentile bins, and confusion matrices were constructed using this discretized format. The diagonal elements of each matrix represent correct predictions within the same percentile bin, while off-diagonal elements indicate misclassification. We computed classification accuracy as the proportion of correct bin assignments:

$$\text{Accuracy} = \frac{\text{Number of correct bin assignments}}{\text{Total number of samples}} \quad (6)$$

Unlike AGILE, which computes accuracy over the entire dataset, we evaluate classification performance strictly on the test set to provide a more realistic estimate of model generalization.

5 Conclusion

This study introduces LANTERN, a comprehensive benchmarking framework for predicting lipid nanoparticle (LNP) transfection efficiency from ionizable lipids. A curated dataset of 1,100 ionizable lipids, derived from experimental HeLa cell transfection measurements, was constructed by correcting label mismatches and removing duplicate SMILES corresponding to geometric isomers from the dataset originally used to train AGILE, the current state-of-the-art regression model in this domain. This refined dataset was used to systematically evaluate a broad spectrum of ML models, including traditional methods, deep neural networks, and graph-based architectures, across multiple molecular feature representations to identify key factors that influence predictive performance in this domain. Our findings show that structure-aware representations, particularly count-based Morgan fingerprints, combined with multi-layer perceptrons, outperform AGILE and other GNN-based models in both accuracy and robustness. These results underscore the importance of thoughtful feature selection, especially in domains constrained by limited data. To facilitate further progress in data-driven LNP design, we release both the refined dataset and the LANTERN library, which enables rapid evaluation and deployment of predictive models for LNP transfection efficiency and beyond. This resource will accelerate the discovery of high-efficiency LNP formulations and support the broader application of ML in molecular property prediction.

Acknowledgment

The authors would like to acknowledge Owen Antholine and Varun Shankar for their valuable assistance with the dataset curation.

References

- [1] Yan, Y. *et al.* Non-viral vectors for rna delivery. *Journal of Controlled Release* **342**, 241–279 (2022).
- [2] Zhu, Y., Zhu, L., Wang, X. & Jin, H. Rna-based therapeutics: an overview and prospectus. *Cell death & disease* **13**, 644 (2022).
- [3] Ibba, M. L., Ciccone, G., Esposito, C. L., Catuogno, S. & Giangrande, P. H. Advances in mrna non-viral delivery approaches. *Advanced drug delivery reviews* **177**, 113930 (2021).
- [4] Kim, M. *et al.* Engineered ionizable lipid nanoparticles for targeted delivery of rna therapeutics into different types of cells in the liver. *Science advances* **7**, eabf4398 (2021).
- [5] Wittrup, A. *et al.* Visualizing lipid-formulated sirna release from endosomes and target gene knockdown. *Nature biotechnology* **33**, 870–876 (2015).
- [6] Xu, E., Saltzman, W. M. & Piotrowski-Daspit, A. S. Escaping the endosome: assessing cellular trafficking mechanisms of non-viral vehicles. *Journal of Controlled Release* **335**, 465–480 (2021).
- [7] Albertsen, C. H. *et al.* The role of lipid components in lipid nanoparticles for vaccines and gene therapy. *Advanced drug delivery reviews* **188**, 114416 (2022).
- [8] Cheng, Q. *et al.* Selective organ targeting (sort) nanoparticles for tissue-specific mrna delivery and crispr-cas gene editing. *Nature nanotechnology* **15**, 313–320 (2020).
- [9] Ni, H. *et al.* Piperazine-derived lipid nanoparticles deliver mrna to immune cells in vivo. *Nature Communications* **13**, 4766 (2022).
- [10] Gan, Z. *et al.* Nanoparticles containing constrained phospholipids deliver mrna to liver immune cells in vivo without targeting ligands. *Bioengineering & translational medicine* **5**, e10161 (2020).
- [11] Qiu, M. *et al.* Lung-selective mrna delivery of synthetic lipid nanoparticles for the treatment of pulmonary lymphangioleiomyomatosis. *Proceedings of the national academy of sciences* **119**, e2116271119 (2022).
- [12] Zhu, Y. *et al.* Multi-step screening of dna/lipid nanoparticles and co-delivery with sirna to enhance and prolong gene expression. *Nature communications* **13**, 4282 (2022).
- [13] Li, B. *et al.* Combinatorial design of nanoparticles for pulmonary mrna delivery and genome editing. *Nature biotechnology* **41**, 1410–1415 (2023).
- [14] Liu, S. *et al.* Membrane-destabilizing ionizable phospholipids for organ-selective mrna delivery and crispr-cas gene editing. *Nature materials* **20**, 701–710 (2021).
- [15] Liu, S. *et al.* Zwitterionic phospholipidation of cationic polymers facilitates systemic mrna delivery to spleen and lymph nodes. *Journal of the American Chemical Society* **143**, 21321–21330 (2021).
- [16] Radmand, A. *et al.* The transcriptional response to lung-targeting lipid nanoparticles in vivo. *Nano letters* **23**, 993–1002 (2023).
- [17] Radmand, A. *et al.* Cationic cholesterol-dependent lnp delivery to lung stem cells, the liver, and heart. *Proceedings of the National Academy of Sciences* **121**, e2307801120 (2024).
- [18] Miao, L. *et al.* Delivery of mrna vaccines with heterocyclic lipids increases anti-tumor efficacy by sting-mediated immune cell activation. *Nature biotechnology* **37**, 1174–1185 (2019).
- [19] Li, B. *et al.* Accelerating ionizable lipid discovery for mrna delivery using machine learning and combinatorial chemistry. *Nature Materials* 1–7 (2024).
- [20] Han, X. *et al.* An ionizable lipid toolbox for rna delivery. *Nature communications* **12**, 7233 (2021).
- [21] Ding, D. Y., Zhang, Y., Jia, Y. & Sun, J. Machine learning-guided lipid nanoparticle design for mrna delivery. *arXiv preprint arXiv:2308.01402* (2023).
- [22] Moayedpour, S. *et al.* Representations of lipid nanoparticles using large language models for transfection efficiency prediction. *Bioinformatics* btae342 (2024).
- [23] Rong, Y. *et al.* Self-supervised graph transformer on large-scale molecular data. *Advances in neural information processing systems* **33**, 12559–12571 (2020).
- [24] Duvenaud, D. K. *et al.* Convolutional networks on graphs for learning molecular fingerprints. *Advances in neural information processing systems* **28** (2015).
- [25] Irwin, R., Dimitriadis, S., He, J. & Bjerrum, E. J. Chemformer: a pre-trained transformer for computational chemistry. *Machine Learning: Science and Technology* **3**, 015022 (2022).

- [26] Xu, Y. *et al.* Agile platform: a deep learning powered approach to accelerate lnp development for mrna delivery. *Nature communications* **15**, 6305 (2024).
- [27] Wang, Y., Wang, J., Cao, Z. & Barati Farimani, A. Molecular contrastive learning of representations via graph neural networks. *Nature Machine Intelligence* **4**, 279–287 (2022).
- [28] Chen, T., Kornblith, S., Norouzi, M. & Hinton, G. A simple framework for contrastive learning of visual representations. In *International conference on machine learning*, 1597–1607 (PMLR, 2020).
- [29] Rogers, D. & Hahn, M. Extended-connectivity fingerprints. *Journal of Chemical Information and Modeling* **50**, 742–754 (2010). URL <https://doi.org/10.1021/ci100050t>. PMID: 20426451, <https://doi.org/10.1021/ci100050t>.
- [30] Landrum, G. Rdkit: Open-source cheminformatics. *Online* **1** (2013).
- [31] Riniker, S. & Landrum, G. A. Better informed distance geometry: Using what we know to improve conformation generation. *Journal of Chemical Information and Modeling* **55**, 2562–2574 (2015).
- [32] Van der Maaten, L. & Hinton, G. Visualizing data using t-sne. *Journal of machine learning research* **9** (2008).
- [33] Awad, M., Khanna, R., Awad, M. & Khanna, R. Support vector regression. *Efficient learning machines: Theories, concepts, and applications for engineers and system designers* 67–80 (2015).
- [34] Vert, J.-P., Tsuda, K. & Schölkopf, B. 2 a primer on kernel methods. *Kernel Methods in Computational Biology* 35 (2004).
- [35] Moriwaki, H., Tian, Y.-S., Kawashita, N. & Takagi, T. Mordred: a molecular descriptor calculator. *Journal of cheminformatics* **10**, 4 (2018).
- [36] Vaswani, A., Shazeer, N. & et al. Attention is all you need. *Advances in neural information processing systems* **30** (2017).
- [37] Devlin, J., Chang, M.-W., Lee, K. & Toutanova, K. Bert: Pre-training of deep bidirectional transformers for language understanding (2019). 1810.04805.
- [38] Breiman, L. Random forests. *Machine learning* **45**, 5–32 (2001).
- [39] Kramer, O. K-nearest neighbors. *Dimensionality reduction with unsupervised nearest neighbors* 13–23 (2013).
- [40] Heid, E. *et al.* Chemprop: A machine learning package for chemical property prediction. *Journal of Chemical Information and Modeling* **64**, 9–17 (2024). URL <https://doi.org/10.1021/acs.jcim.3c01250>. PMID: 38147829, <https://doi.org/10.1021/acs.jcim.3c01250>.
- [41] Li, H. *et al.* A knowledge-guided pre-training framework for improving molecular representation learning. *Nature Communications* **14**, 7568 (2023).
- [42] Belenahalli Shekarappa, S., Kandagalla, S. & Lee, J. Development of machine learning models based on molecular fingerprints for selection of small molecule inhibitors against jak2 protein. *Journal of Computational Chemistry* **44**, 1493–1504 (2023).
- [43] Maggiora, G., Vogt, M., Stumpfe, D. & Bajorath, J. Molecular similarity in medicinal chemistry: miniperspective. *Journal of medicinal chemistry* **57**, 3186–3204 (2014).
- [44] Petrone, P. M. *et al.* Rethinking molecular similarity: comparing compounds on the basis of biological activity. *ACS chemical biology* **7**, 1399–1409 (2012).
- [45] Orosz, Á., Héberger, K. & Rácz, A. Comparison of descriptor-and fingerprint sets in machine learning models for adme-tox targets. *Frontiers in Chemistry* **10**, 852893 (2022).
- [46] Periwal, V. *et al.* Bioactivity assessment of natural compounds using machine learning models trained on target similarity between drugs. *PLoS computational biology* **18**, e1010029 (2022).
- [47] Zagidullin, B., Wang, Z., Guan, Y., Pitkänen, E. & Tang, J. Comparative analysis of molecular fingerprints in prediction of drug combination effects. *Briefings in bioinformatics* **22**, bbab291 (2021).
- [48] Tejera, E. *et al.* Cell fishing: A similarity based approach and machine learning strategy for multiple cell lines-compound sensitivity prediction. *PLoS One* **14**, e0223276 (2019).
- [49] Zhong, S. & Guan, X. Count-based morgan fingerprint: A more efficient and interpretable molecular representation in developing machine learning-based predictive regression models for water contaminants’ activities and properties. *Environmental science & technology* **57**, 18193–18202 (2023).
- [50] Hoerl, A. E. & Kennard, R. W. Ridge regression: Biased estimation for nonorthogonal problems. *Technometrics* **12**, 55–67 (1970).
- [51] Hearst, M., Dumais, S., Osuna, E., Platt, J. & Scholkopf, B. Support vector machines. *IEEE Intelligent Systems and their Applications* **13**, 18–28 (1998).
- [52] Chen, T. & Guestrin, C. Xgboost: A scalable tree boosting system. In *Proceedings of the 22nd acm sigkdd international conference on knowledge discovery and data mining*, 785–794 (2016).
- [53] Prokhorenkova, L., Gusev, G., Vorobev, A., Dorogush, A. V. & Gulin, A. Catboost: unbiased boosting with categorical features. *Advances in neural information processing systems* **31** (2018).
- [54] Zhou, H. & Skolnick, J. Utility of the morgan fingerprint in structure-based virtual ligand screening. *The Journal of Physical Chemistry B* **128**, 5363–5370 (2024).

- [55] Tayyebi, A. *et al.* Prediction of organic compound aqueous solubility using machine learning: a comparison study of descriptor-based and fingerprints-based models. *Journal of Cheminformatics* **15**, 99 (2023).
- [56] Moriwaki, H., Tian, Y.-S., Kawashita, N. & Takagi, T. Moesm4 of mordred: a molecular descriptor calculator. (*No Title*) (2018).
- [57] Seal, S., Yang, H., Vollmers, L. & Bender, A. Comparison of cellular morphological descriptors and molecular fingerprints for the prediction of cytotoxicity-and proliferation-related assays. *Chemical Research in Toxicology* **34**, 422–437 (2021).
- [58] Fang, S., Liu, Y. & Liu, S. Mfgb: molecular properties prediction leveraging self-supervised morgan fingerprint representation learning. In *2023 IEEE International Conference on Bioinformatics and Biomedicine (BIBM)*, 3004–3011 (IEEE, 2023).
- [59] Gaulton, A. *et al.* The chembl database in 2017. *Nucleic acids research* **45**, D945–D954 (2017).
- [60] Mehradfar, A. *et al.* Supervised learning for analog and rf circuit design: Benchmarks and comparative insights. *arXiv preprint arXiv:2501.11839* (2025).
- [61] An, Q., Rahman, S., Zhou, J. & Kang, J. J. A comprehensive review on machine learning in healthcare industry: classification, restrictions, opportunities and challenges. *Sensors* **23**, 4178 (2023).
- [62] Kingma, D. P. & Ba, J. Adam: A method for stochastic optimization (2017). 1412. 6980.
- [63] Ramsundar, B. *et al.* *Deep Learning for the Life Sciences* (O'Reilly Media, 2019). <https://www.amazon.com/Deep-Learning-Life-Sciences-Microscopy/dp/1492039837>.

Supplementary Information

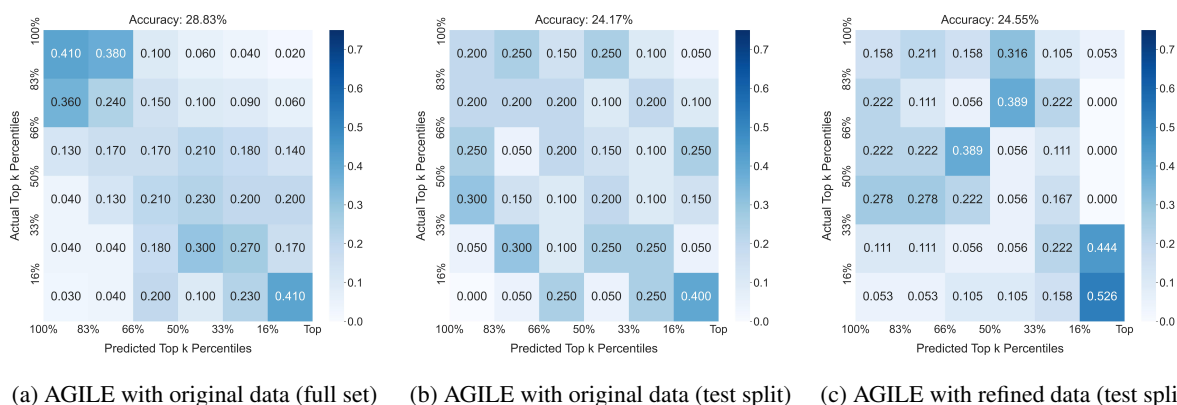


Figure S1: **Confusion matrices for the AGILE model under different data conditions.** (a) AGILE trained on the original 1200-point dataset, with the confusion matrix computed over the entire dataset (train, validation, and test), as presented in the AGILE study [26]. (b) The same AGILE model as in (a), but the confusion matrix is computed only on the test split of the original dataset. (c) AGILE trained on the refined 1100-point dataset with Murcko scaffold-based splitting, with the confusion matrix computed on its test split. The differences highlight the impact of dataset refinement on model predictions.

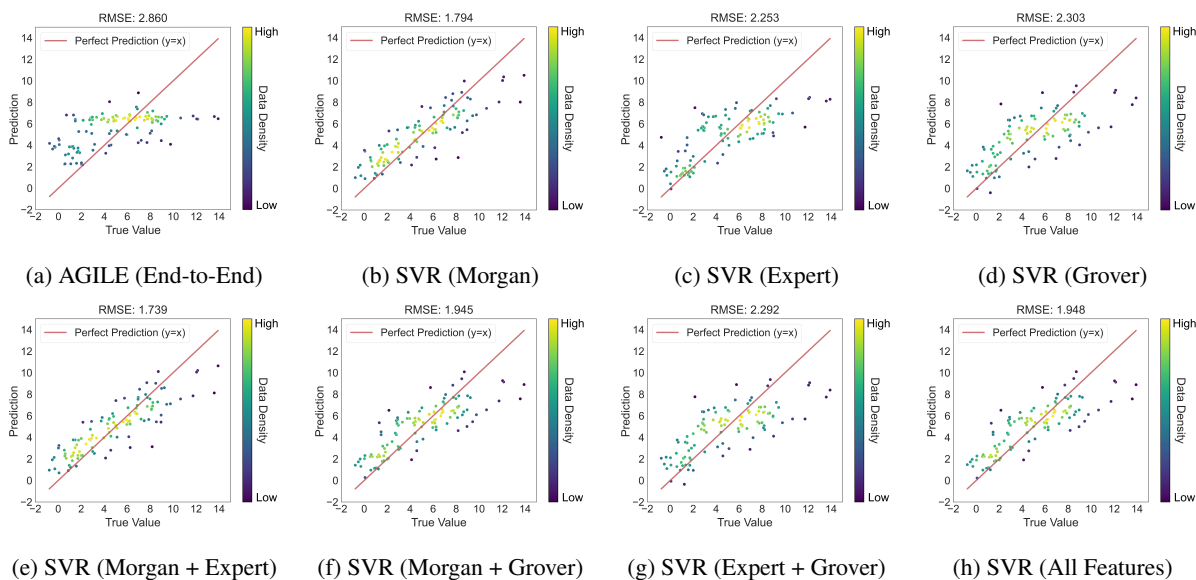


Figure S2: **Prediction vs. true value plots for different feature sets.** (a) AGILE model using end-to-end features. (b–h) SVR model trained with different feature sets, including Morgan, Expert, and Grover representations individually and in combination. *Morgan fingerprints* combined with *Expert descriptors* yield the best performance with the lowest RMSE, reinforcing the effectiveness of integrating domain-specific knowledge with substructure-based representations.

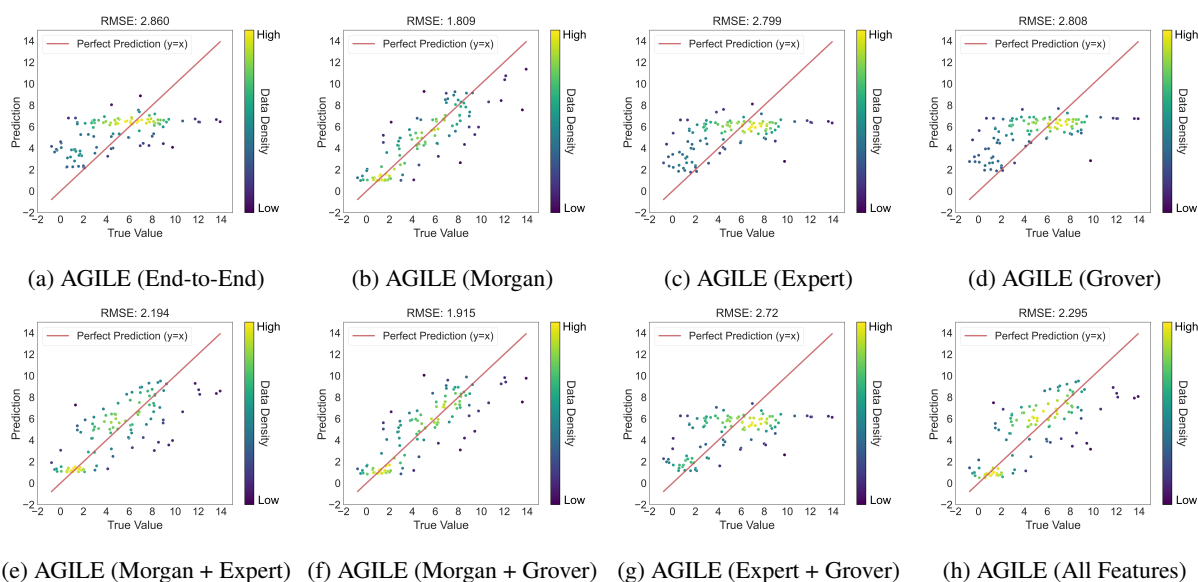


Figure S3: **Prediction vs. true value plots for different feature sets in AGILE.** (a) AGILE model using only its end-to-end learned features. (b–h) AGILE model incorporating additional feature sets alongside its end-to-end representations, including Morgan, Expert, and Grover embeddings individually and in various combinations. *Morgan fingerprints* provide the most significant improvement in predictive accuracy, demonstrating their effectiveness in enhancing AGILE’s performance.

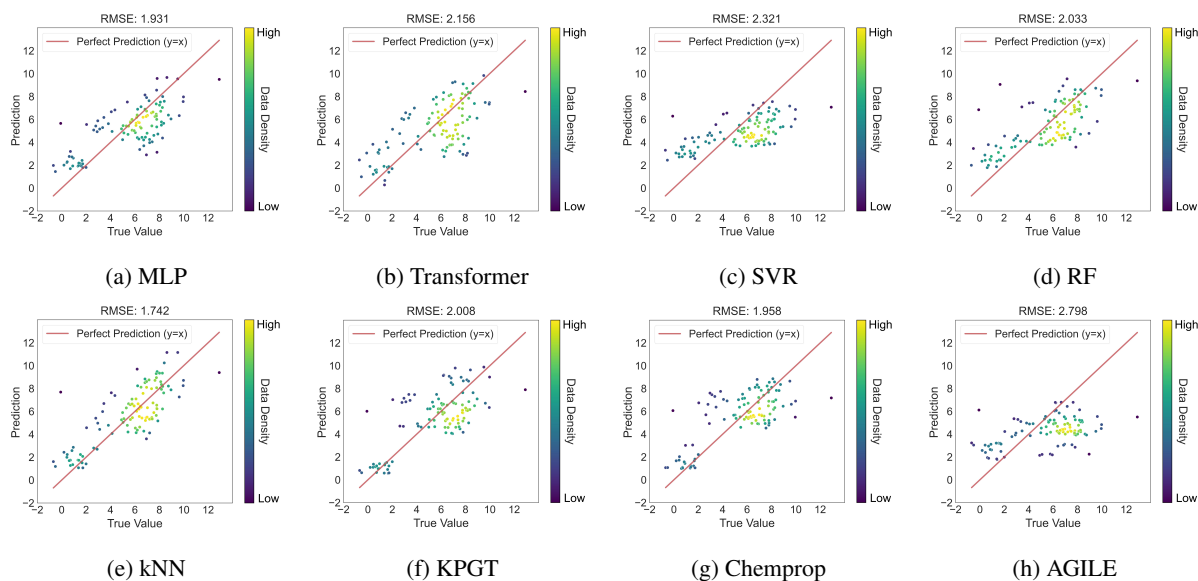


Figure S4: **Prediction vs. true value plots for different models using Murcko scaffold split.** Each plot presents the best-performing feature set for the corresponding model, selected based on Table 3. (a–h) show the predictive performance of MLP, Transformer, SVR, RF, kNN, KPGT, Chemprop, and AGILE, respectively. Compared to the random split case, most models exhibit a drop in predictive accuracy due to the more stringent generalization requirements of the scaffold-based split. However, kNN and Chemprop maintain similar performance levels, indicating their robustness to distribution shifts, while other models, including MLP and SVR, experience a noticeable decline. AGILE continues to show the lowest accuracy.